International Journal of Applied Engineering Research
ISSN 0973-4562 Volume 10, Number 6 (2015) pp. 15251-15266

http://www.ripublication.com

A Numerical Investigation on Performance Enhancement of Air Motor Using Computational Fluid Dynamics

Aezhisai Vallavi. M.S[1], Kiranlal.S[2] and Mohandas Gandhi.N[3]
[1]Department of Mechanical Engineering, Kumaraguru College of Technology, Coimbatore, Tamilnadu, India
[2]P.G Scholar, Kumaraguru College of Technology, Coimbatore, Tamilnadu, India
[3]Principal, Kalaignar Karunanithi Institute of Technology, Coimbatore, Tamilnadu, India
Email: kiranlal2211@gmail.com

Abstract

Modern industry uses computational methodology to great extent and these methodologies reduces cost, time and reduces the difficulties involved in experimental testing procedures. With the exceptional advantages like having insight, fore-sight computational methodologies almost take over experimental techniques when the later become impossible in many cases. In this work computational fluid dynamics (CFD) is utilized to understand the inherent complex hydrodynamic behavior of rotor-casing interaction and its influence on the power and torque characteristics of the air motor. A parametric study is executed using one of the design of experiments(DOE) techniques called Taguchi method, by varying different parameters such as number of vanes, injection angle at inlet and blade inclination angle and optimum configuration is achieved at the pressure of 4.2 bar at 2000rpm.

Key Words: CFD, DOE, Injection angle, Blade inclination angle, Vane, Air motors.

Introduction

A vane type air motor uses compressed air to produce rotational motion to a shaft. A slotted rotor which is mounted on a drive shaft is the rotating element. A freely sliding rectangular vane is fitted to each slot of the rotor. The rotor and vanes are enclosed inside the stator. The rotor is mounted eccentric to the stator. When the rotor is in motion, the vanes tend to slide outward due to centrifugal force. The number of vanes and the ratio of stator to rotor diameter may vary according to the air motor performance. The vanes are held on to the inner surface of the stator by means of

springs. When compressed air is directed into the inlet port, its pressure is exerted equally in all directions.

A new concept of the air engine using compressed air as the potential power source for motorbikes, in place of an internal combustion engine is proposed by Bharat Raj Singh [2]. The maximum power output is obtained as 3.977kW at the different rotor to casing diameter ratios, optimal injection angle 60◦, vane angle 45◦ for linear expansion (i.e., at minimum air consumption) when the casing diameter is kept 100 mm, at injection pressure 6 bar (90 psi) and speed of rotation 2500 rpm. Later the effect of isobaric admission and adiabatic expansion of high pressure air for different rotor to casing diameter ratios at optimum number of vanes and injection angles was studied and analyzed [5] Anirudh Addala et al [7] used compressed air as the working medium in car. They concluded that air motor provides the required thrust to propel the car and also very economical. A complete dynamic process of the air motor system is derived based on the mechanical structure, orifice and other physics theory. Bharat Raj Singh et al [11] analyzed the critical effect of rotor vanes with different injection angles on performance of a vaned type novel air turbine. They have concluded that the total shaft power is found optimum at injection angle 60° when there are 10 vanes , for injection pressure 6 bar and speed of rotation 2500 rpm. Bharat Raj Singh et al [12] concludes that The optimum power output is seen to be 7.645 kW at 0.80 rotor/ casing ratio for injection pressure of 6 bar. Onkar Singh et al [1] studied the effect of rotor to casing ratios with different rotor vanes on performance of shaft output of a vane type novel air turbine and In that study, the maximum power is obtained as 4.5kW - 5.3kW when 100 mm is taken as casing diameter , and rotor to casing diameter ratios are kept from 0.65 to 0.55. Xing Luo et al [8] developed a mathematical model for vane-type air motors with arbitrary n vanes and concluded that The continuous approximation provide control engineers a continuous working model to develop control strategy using advance control methods. In this paper air motor for the application of hoist is modeled and analyzed. A hoist will be used to lift materials to the roof of a building during construction. Variable speed is needed because of the variety of articles to be lifted. The hoist should operate at a construction sites in all kinds of weather and electricity may not be readily available at all times. An air motor is a good choice for the variable-speed requirement, weather conditions, and lack of electricity. The air motor can provide the variable horsepower needed with the change in load.

Model Generation

Geometrical details

The dimensions for the Air motor model used in this analysis is obtained from Gast Manufacturing, Inc. in this model the casing diameter is 71mm and rotor to casing diameter ration is 0.90. Modeling is done using CATIA V5 software. The corresponding Experimental data performance curve is given in the figure 2 and CATIA model is shown in figure 1.

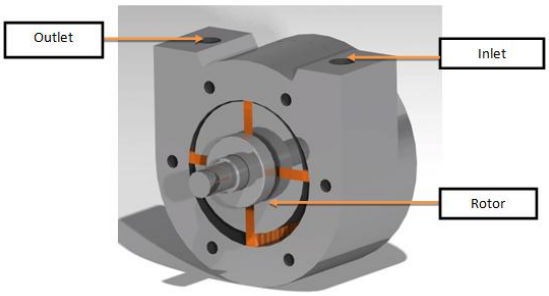

Figure 1: Air motor model-CATIA

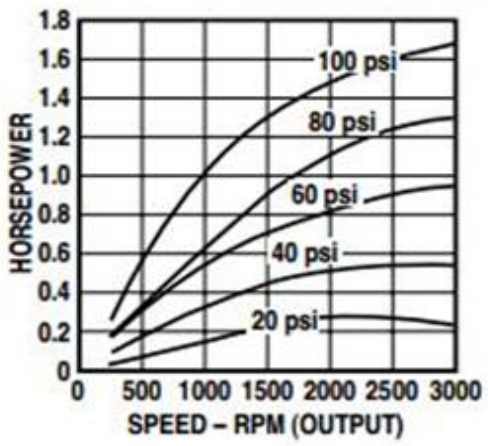

(a)

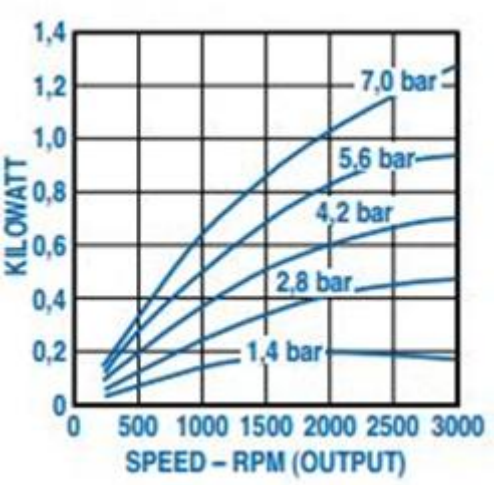

(b)

Figure 2: Performance curve-Power VS Speed

The graph between the speed and the power gives the performance data. At the pressure of 1.4 bar the output power will be 0.14, 0.2, 0.18 at the speed of 1000, 2000 and 3000 rpm respectively. At the pressure of 4.2 bar the power obtained at the respective rpm is 0.38, 0.6 and 0.7.

Numerical Methodology

Domain Discretization/Meshing

Due to the complexity of geometry the surface is discretized with tri elements. These tri elements are created in such a way that they capture the boundaries to a possible better accuracy. The maximum equiangular skewness for surface mesh is kept as0.6 and 0.9 for volume mesh elements .The Surface mesh of the air motor is generated in Automatic Net generation for Structural Analysis (ANSA) (as shown in the figure). The volume mesh is generated in T-Grid.

Mesh quality and skewness

This quality criteria for mesh applies to all cells and face shapes and is almost always used for prisms and pyramids.

Skewness (for a quad) = $\max\left[\frac{\theta_{max}-90}{90}, \frac{90-\theta_{max}}{90}\right]$ …….(1)

Equiangular skew, another common measure of quality is based on equiangular skew.

Equivalent skew = $\max\left[\frac{\theta_{max}-\theta_0}{180-\theta_0}, \frac{\theta_0-\theta_{max}}{\theta_0}\right]$ ……(2)

where,

θ_{max} the largest angle in a face or cell,

θ_0 is the angle for equi-angular face or cell i.e. 60 degree for a triangle and 90 degree for a square.

A Skewness of zero is the best possible one and a skewness of one is almost never preferred. For Hexagonal and quadratic cells, skewness should not exceed 0.85 in order to obtain accurate solution. Skewness should not exceed 0.85 and 0.9 for triangular and tetragonal cells respectively.

Solver Setup

- Three dimensional, incompressible and turbulent flow is assumed.
- Moving reference frame (MRF) is used to model the moving parts (rotor)
- Pressure-velocity coupling is done by segregated method.
- SIMPLE (semi implicit pressure linked equation) algorithm is used
- Second order discretization scheme is used for solving the pressure and momentum equations.

Governing Equations

The basic governing equations for fluid flow are conservation of mass and momentum. These equations describe the behavior of fluids. The flow behavior is assumed to be incompressible, turbulent in nature. The rotating rotor is solved using moving reference frame with constant rotational speed equal to whereas the flow through the stationary parts like casing is solved using inertial frame of reference.

Moving Reference Frame (MRF)

The air motor has both rotating and stationary components, which are coupled together in a CFD model by one or two interface models. The multiple reference frame (MRF) technique is one such interface model. In stationary frame of reference N-S equations are solved for absolute velocities and in moving reference frame the same N-S equations are solved for relative velocities.

For three-dimensional incompressible and steady flow, the continuity equation and momentum equation:

For Stationary part:

Continuity Equation:

$$\frac{\partial u}{\partial x}+\frac{\partial \nu}{\partial y}+\frac{\partial w}{\partial z}=0 \text{.....(3)}$$

X-momentum:

$$\rho\left[U\frac{\partial u}{\partial x}+V\frac{\partial u}{\partial y}+W\frac{\partial u}{\partial z}\right]=-\frac{\partial p}{\partial x}+\mu\left[\frac{\partial^2 u}{\partial x^2}+\frac{\partial^2 u}{\partial y^2}+\frac{\partial^2 u}{\partial z^2}\right] \quad \text{……..(4)}$$

Y-momentum:

$$\rho\left[U\frac{\partial v}{\partial x}+V\frac{\partial v}{\partial y}+W\frac{\partial v}{\partial z}\right]=-\frac{\partial p}{\partial y}+\mu\left[\frac{\partial^2 v}{\partial x^2}+\frac{\partial^2 v}{\partial y^2}+\frac{\partial^2 v}{\partial z^2}\right] \quad \text{…….(5)}$$

Z-momentum:

$$\rho\left[U\frac{\partial w}{\partial x}+V\frac{\partial w}{\partial y}+W\frac{\partial w}{\partial z}\right]=$$
$$-\frac{\partial p}{\partial z}+\mu\left[\frac{\partial^2 w}{\partial x^2}+\frac{\partial^2 w}{\partial y^2}+\frac{\partial^2 w}{\partial z^2}\right]\ldots \quad \ldots(6)$$

For Moving part:

X-momentum:

$$\rho\left[U_r\frac{\partial u_r}{\partial x}+V_r\frac{\partial u_r}{\partial y}+W_r\frac{\partial u_r}{\partial z}\right]=$$
$$-\frac{\partial p}{\partial x}+\mu\left[\frac{\partial^2 u_r}{\partial x^2}+\frac{\partial^2 u_r}{\partial y^2}+\frac{\partial^2 u_r}{\partial z^2}\right] \quad \ldots\ldots(7)$$

Y-momentum:

$$\rho\left[U_r\frac{\partial v_r}{\partial x}+V_r\frac{\partial v_r}{\partial y}+W_r\frac{\partial v_r}{\partial z}\right]=$$
$$-\frac{\partial p}{\partial x}+\mu\left[\frac{\partial^2 v_r}{\partial x^2}+\frac{\partial^2 v_r}{\partial y^2}+\frac{\partial^2 v_r}{\partial z^2}\right] \quad \ldots\ldots(8)$$

Z-momentum:

$$\rho\left[U_r\frac{\partial w_r}{\partial x}+V_r\frac{\partial w_r}{\partial y}+W_r\frac{\partial w_r}{\partial z}\right]=$$
$$-\frac{\partial p}{\partial x}+\mu\left[\frac{\partial^2 w_r}{\partial x^2}+\frac{\partial^2 w_r}{\partial y^2}+\frac{\partial^2 w_r}{\partial z^2}\right] \quad \ldots..(9)$$

Boundary and Cell Zone Conditions

To define any CFD problem properly the term boundary condition and cell zone is very important. Any numerical problem is of boundary value problem or initial value problem or mixed type. For this type of problem all the boundary has to be applied with certain boundary condition. They may be of Dirichlet condition or Neumann boundary condition or mixed type. With these boundary conditions only the value at the inner nodes are calculated. Cell zone condition defines the nature of the cell whether it is fluid or solid.

Table 1: Boundary and Cell Zone Conditions

Parameters	Computational Fluid Dynamics (CFD)
Fluid	Air at 25°C
Inlet	Pressure inlet
Outlet	Pressure outlet
Density	1.22 kg/m3
Viscosity	1.7894e-5 kg/ms
Turbulence Model	K-ε Realizable Model

Modeling Turbulence

Turbulence is modeled through Realizable k-ε Model as it has the capability to capture complex rotor-casing interaction. The modeled transport equations for k and ε in the realizable k –ε Model are,

$$\frac{\partial}{\partial t}(\rho k)+\frac{\partial}{\partial x_i}(\rho k u_i)=$$
$$\frac{\partial}{\partial x_j}\left[\left(\mu+\frac{\mu_t}{\sigma_k}\right)\frac{\partial k}{\partial x_j}\right]+G_K+G_b-\rho\epsilon-Y_M+S_K$$

and

$$(\rho\varepsilon)+\frac{\partial}{\partial x_i}(\rho\varepsilon u_i)=\frac{\partial}{\partial x_j}\left[\left(\mu+\frac{\mu_t}{\sigma_\varepsilon}\right)\frac{\partial \varepsilon}{\partial x_i}\right]+\rho C_1 S\varepsilon$$
$$\rho C_2\frac{\varepsilon^2}{k+\sqrt{v\varepsilon}}+C_{1\varepsilon}\frac{\varepsilon}{K}C_{3\varepsilon}G_b+S_\varepsilon$$
$$C_1=max\left[0.43\frac{\eta}{\eta+5}\right],\eta=S\frac{K}{\varepsilon},S=\sqrt{2S_{ij}S_{ij}}$$

In these equations, G_k represents the generation of turbulence kinetic energy due to the mean velocity gradients, calculated as described in modeling turbulent production in the k-ε models. G_b is the generation of turbulence kinetic energy due to buoyancy, calculated as described in effects of buoyancy on turbulence in the k-ε models, Y_M represents the contribution of the fluctuating dilatation in compressible turbulence to the overall dissipation rate, calculated as described in effects of compressibility on turbulence in the k-ε models. C_2 and $C_{1\varepsilon}$ are constants. σ_K and σ_ε are the turbulent Prandtl numbers for k and ε ,respectively. S_K and S_ε are user-defined source terms.

Validation Study

Though computational methodology has so many advantages still there are certain variables on which the numerical results rely upon. They are mesh count, mesh size/shape, turbulence models and numerical algorithms. Hence any computational procedure is problem specific. Thus it is important for CFD user to find the optimum computational methodology to solve certain problem.

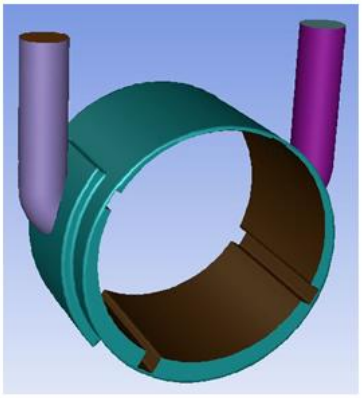

Figure 3: Fluid domain extraction-base model

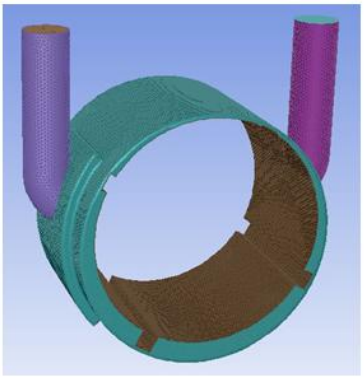

Figure 4: Meshed model

CFD Results for various mesh counts ranging from 0.21388 million to 0.62217 million are obtained and it was found that at a mesh count of 0.577570 computational results attained grid independence. That is after this mesh count any further increase in mesh has no considerable variation in CFD results. Various turbulence models starting from Spallart-Allmaras,K, K-ε, K-ω and their sub variants are tried and it is found K-ε realizable model gives better accuracy than all other models. Comparative results for K-ε realizable model with 0.577570 mesh count and second-order numerical algorithm (CFD) to experimental power is shown in figure.

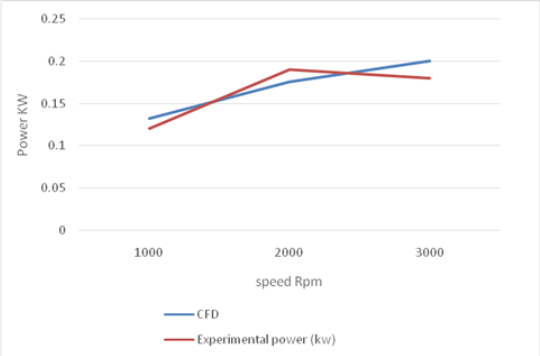

Figure 5: Experimental result VS CFD result (1.4 bar pressure)

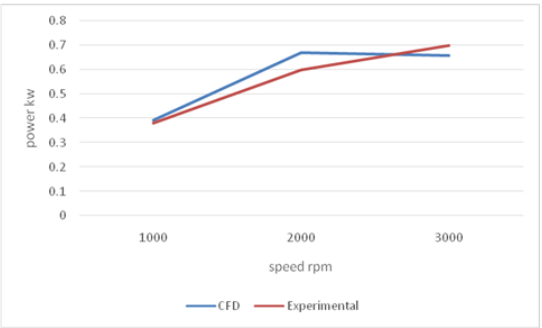

Figure 6: Experimental result VS CFD result (4.2 bar pressure)

It is found there is a good agreement between CFD and experimental results with the maximum discrepancy less than 5%.Thus this computational methodology is to be applied to further performance enhancement study.

Performance Enhancement Study

This chapter deals in enhancing the performance of air motor by changing its geometrical configuration. Three variables such as number of vanes, blade inclination angle and injection angle are considered for design modification. Three levels of these variables are considered. With three variables at three levels the number of combinations reaches more and the number of experiments also become very more.

To avoid number of trials a well devised mathematical DOE tool has to be applied. Being simple and efficient Taguchi method, one of the Design of Experiments methods is used for the performance enhancement study.

Table 2: Basic Taguchi table

For variable = 3, level=3				
Run#	A	B	C	X
1 2 3	1 1 1	1 2 3	1 2 3	X1 X2 X3
4 5 6	2 2 2	1 2 3	2 3 1	X4 X5 X6
7 8 9	3 3 3	1 2 3	3 1 2	X7 X8 X9

Table 3: Taguchi table for Performance Enhancement study

Number of vanes	Blade inclination angle	Injection angle	Modification
4 4 4	90 30 45	25 30 35	Base model M1 M2
6 6 6	90 30 45	30 35 25	M3 M4 M5
8 8 8	90 30 45	35 25 30	M 6 M 7 M8

Table 4: Performance Enhancement study

Description	Model	Mesh	Mesh parameters
Modification 1	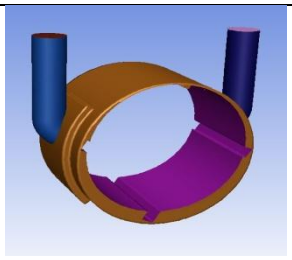	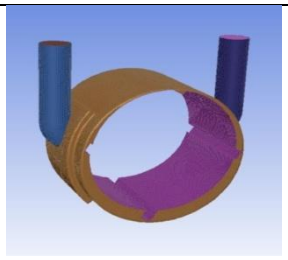	Surface mesh count: 777725 Volume mesh count: 500694 Surface mesh Skewness: 0.64 Volume mesh quality: 0.84

Modification 2	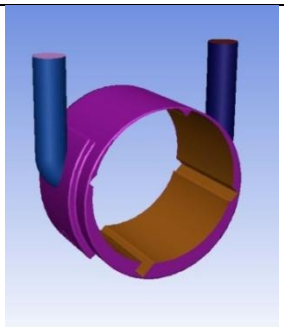	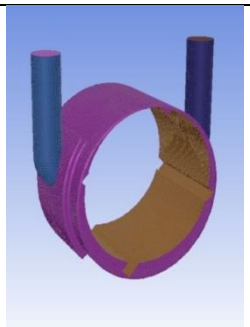	Surface mesh count: 77049 Volume mesh count: 510247 Surface mesh Skewness: 0.578 Volume mesh quality: 0.81
Modification 3	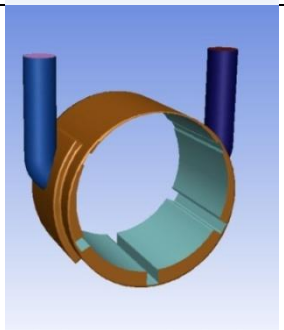	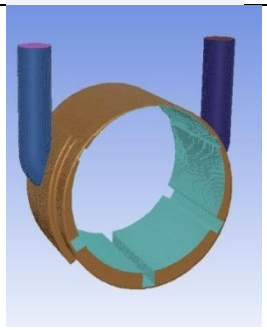	Surface mesh count: 79547 Volume mesh count: 511864 Surface mesh Skewness: 0.609 Volume mesh quality:0.83
Modification 4	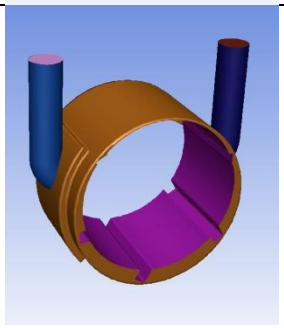	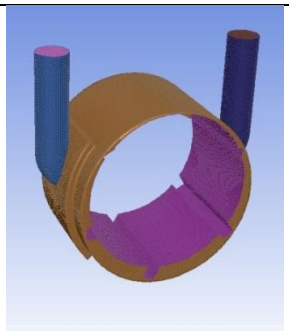	Surface mesh count: 79606 Volume mesh count: 519769 Surface mesh Skewness: 0.66 Volume mesh quality: 0.81
Modification 5	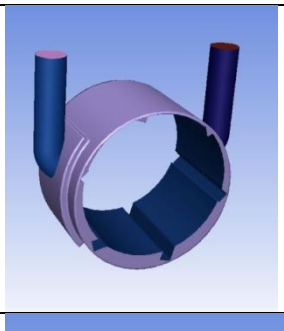	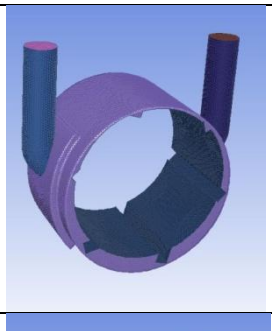	Surface mesh count: 78637 Volume mesh count: 509670 Surface mesh Skewness: 0.71 Volume mesh quality: 0.84
Modification 6	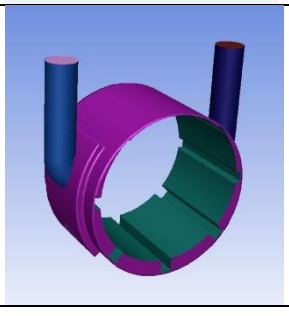	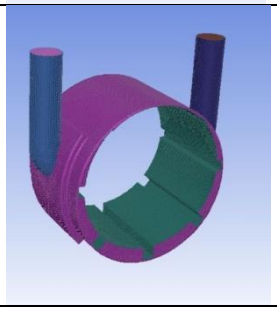	Surface mesh count: 80180 Volume mesh count: 513084 Surface mesh Skewness: 0.68 Volume mesh quality: 0.81

Modification 7	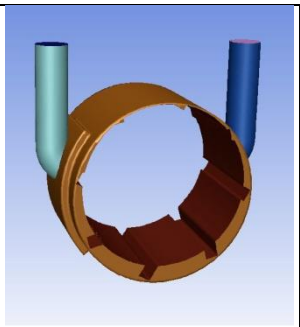	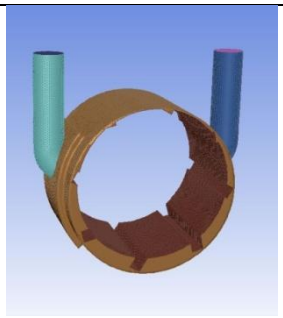	Surface mesh count: 79813 Volume mesh count: 508356 Surface mesh Skewness: 0.72 Volume mesh quality: 0.82
Modification 8	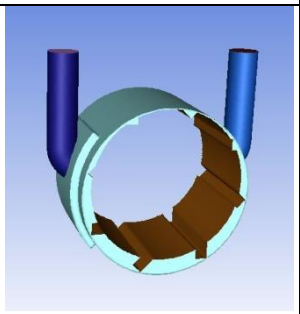	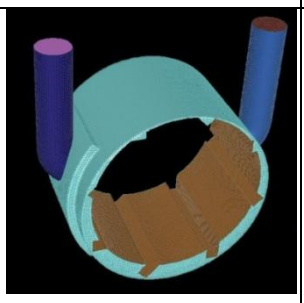	Surface mesh count: 83565 Volume mesh count: 514112 Surface mesh Skewness: 0.678 Volume mesh quality: 0.84

CATIA V5 software is used for modelling and Ansa 13.2.3 is used for surface meshing and surfaces are discretized with tri elements. Volume meshing is done using T-Grid which is one of the volume meshing software .Surface and volume mesh count and quality values are listed above.

Results and Discussion

Table 5: Results

	Inlet pressure (bar)	Speed (rpm)	Torque (Nm)	Power (KW)
Base case	1.4	1000	1.26	0.13188
		2000	0.84	0.175
		3000	0.76	0.2
	4.2	1000	3.75	0.392
		2000	3.2	0.66986667
		3000	2.1	0.6594
M1	4.2	1000	5	0.52333333
		2000	11.6	0.61986667
		3000	3	0.942
M2	4.2	1000	9	0.942
		2000	13	0.72133333
		3000	3	0.942
M3	4.2	1000	6.6	0.6908

		2000	18	0.768
		3000	3.5	1.099
M4	4.2	1000	5.5	0.57566667
		2000	13.5	0.826
		3000	4.4	1.3816
M5	4.2	1000	6	0.628
		2000	14.9	0.80906667
		3000	2.3	0.7222
M6	4.2	1000	3.36	0.35168
		2000	17.9	0.74706667
		3000	3.17	0.99538
M7	4.2	1000	7.55	0.79023333
		2000	18.4	0.85173333
		3000	5.1	1.6014
M8	4.2	1000	8.3	0.86873333
		2000	12.8	0.67946667
		3000	6.1	1.9154

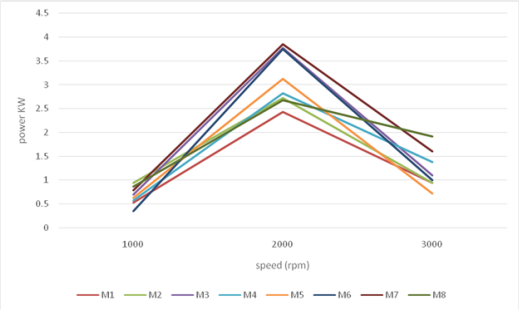

Figure 7: Power VS speed (pressure 4.2 bar)

Above figure 7 shows comparison between various modifications, from that we obtained modification 7 (M7) produce comparably maximum power at a speed of 2000 rpm.

Contour Plots For Base Model

The contours of pressure and velocity for base model and Modification 7 are given in the figure below.

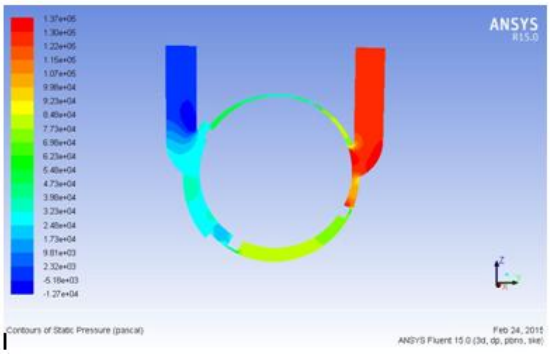

Figure 8: Contours of Static pressure

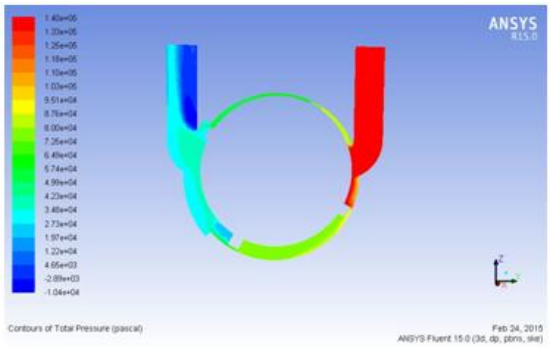

Figure 9: Contours of Total pressure

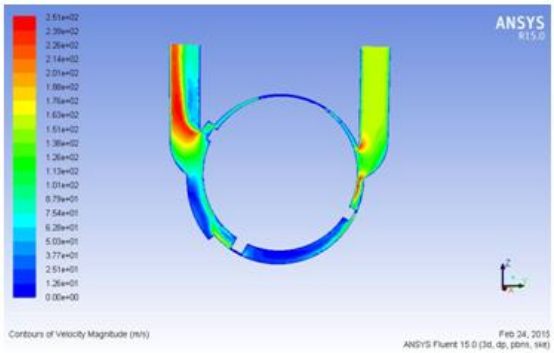

Figure 10: Contours of Velocity magnitude

Contour Plots For Base Model And M7

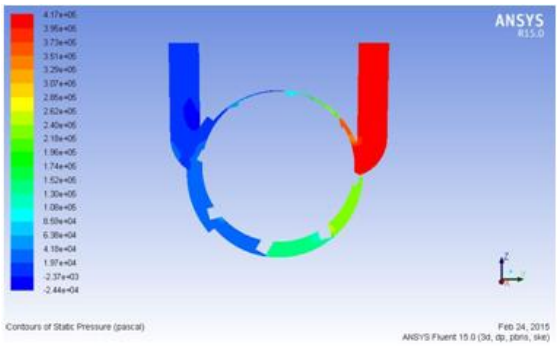

Figure 11: Contours of Static Pressure (M7)

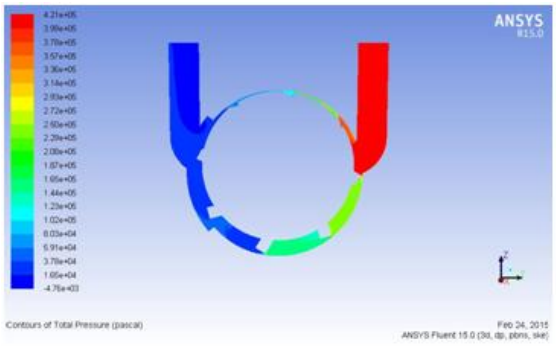

Figure 12: Contours of Total Pressure (M7)

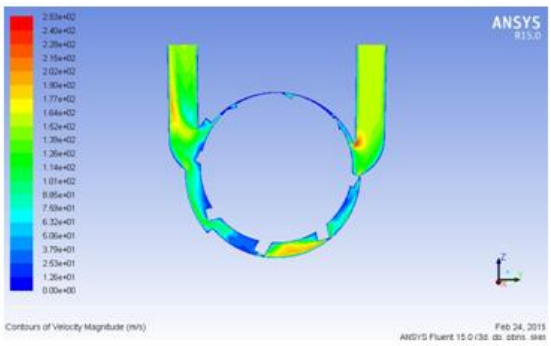

Figure 13: Contours of Velocity Magnitude (M7)

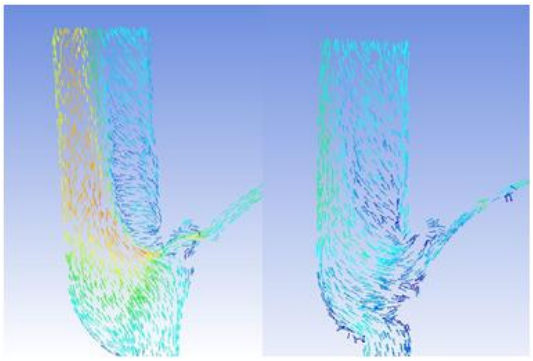

Figure 14: Velocity vector comparison for base model and M7

From the contour plots it is seen that comparing to base model, Model 7 has high static and total pressure .This induces higher torque in turn higher power values. Figure 14 shows orientation of velocity vectors for base model and Modification7.In base model higher velocity values are found at one end and this causes flow recirculation on the neighboring region. This is absent in modification 7.Most of the fluid is oriented towards outlet in modification 7 comparing to base model. More over these high velocity particles increases high head losses as head loss is a function of velocity. As consequence of this power and torque reduces in base model whereas keeping velocity value optimum head loss is minimized in modification 7.

Conclusion

Thus a novel approach is taken to optimize the hydrodynamic performance of air motor is attempted through CFD. The optimum computational procedure with appropriate mesh count, turbulence model and discretization algorithm are found out from the validation study. This procedure is utilized in performance enhancement study. From all the model configuration compared, modification 7 with Number of vanes 8, Blade Inclination angle 30° and Injection angle 25° was found to be the optimum model with increased power.

Reference

[1] Bharat Raj Singh., Onkar Singh., 2010, " Effect of Rotor to Casing Ratios with Different Rotor Vanes on Performance of Shaft Output of a Vane Type Novel Air Turbine," World Academy of Science, Engineering and Technology. , Vol 4.

[2] Bharat Raj Singh., Onkar Singh., 2012, " A Study of Performance Output of a Multivane Air Engine Applying Optimal Injection and Vane Angles," International Journal of Rotating Machinery.

[3] Yu-Ta Shen., Yean-Ren Hwang. , 2012 , "Development of a Novel Pneumatic Hybrid Engine," World Academy of Science, Engineering and Technology., Vol 6.

[4] Dein Shaw., Jyun-Jhe Yu ., Cheng Chieh., 2013, " Design of a Hydraulic Motor System Driven by Compressed Air," Energies.

[5] Bharat Raj Singh., Onkar Singh., 2009, "Theoretical Investigations on Different Casing and Rotor Diameters Ratio to Optimize Shaft Output of a Vaned Type Air Turbine," International Journal of Natural Sciences and Engineering, Vol 1.

[6] Bharat Raj Singh., Onkar Singh., 2011, " Compressed air energy storage system based engine for running light vehicle," International Journal of Energy and Environmental Engineering, Vol 2.

[7] Anirudh Addala., Srinivasu Gangada., 2013, " Fabrication and Testing of Compressed Air Car Viswanadha Institute of Technology and Management," Global Journal of researches in engineering Mechanical and mechanics engineering , Vol 13 , Issue 1 , Version 1.0.

[8] Xing Luo., Jihong Wang., Leonid Shpanin., Nan Jia., Gang Liu., Alan S. I. Zinober., 2008, "Development of a Mathematical Model for Vane-type Air Motors with Arbitrary N Vanes," Proceedings of the World Congress on Engineering.

[9] Abhishek Lal., 2013, "Design and Dynamic Analysis of Single Stroke Compressed Air Engine," International journal of renewable energy research, Vol 3.

[10] Yadav, J, P., Bharat Raj Singh, 2011, " Study and Fabrication of Compressed Air Engine," JPSET, Vol 2.

[11] Bharat Raj Singh ., Onkar Singh., 2010, "Critical Effect of Rotor Vanes with Different Injection Angles on Performance of a Vaned Type Novel Air Turbine," International Journal of Engineering and Technology, Vol 2.

[12] Bharat Raj Singh., Onkar Singh., "Analytical Evaluations of Shaft Output on Different Rotor to Casing Diameter Ratios at Optimal Value of Vane and Injection Angles for a Multi-Vane Air Turbine," JPSET, Vol 1.